Interference effects in the decay of the $3d \rightarrow 5p, 6p$ excitations of Kr studied with fluorescence spectroscopy

A. Sankari,[1,2,*] R. Sankari,[2] S. Heinäsmäki,[1] S. Aksela,[1] H. Aksela,[1] A. Kivimäki,[3] M. Coreno,[4] M. de Simone,[3] and K. C. Prince[5,3]

[1]*Department of Physical Sciences, University of Oulu, P. O. Box 3000, 90014 Oulu, Finland*

[2]*Department of Physics, University of Turku, 20014 Turku, Finland*

[3]*CNR-INFM, TASC Laboratory, 34012 Trieste, Italy*

[4]*CNR-IMIP, Monterotondo, 00016 Roma, Italy*

[5]*Sincrotrone Trieste, AREA Science Park, 34012 Trieste, Italy*

(Received 28 November 2007; revised manuscript received 25 January 2008; published 20 March 2008)

The energy dependence of the fluorescence intensity from the $4p^4(^1D)5p$ states of Kr was studied experimentally across the $3d_{5/2}^{-1}5p$, $3d_{3/2}^{-1}5p$, and $3d_{5/2}^{-1}6p$ resonances. The results of multiconfiguration Dirac-Fock calculations were compared with the measurements and with earlier calculations. The calculated interference effects in the resonant Auger process were found to be very sensitive to the initial state configuration interaction. The addition of the $7p$ orbital in the wave functions did not improve the agreement between experiment and calculation. The effects of cascade processes were also considered with the help of Hartree-Fock calculations.

DOI: 10.1103/PhysRevA.77.032720 PACS number(s): 32.80.Hd, 32.80.Fb

I. INTRODUCTION

The photoexcitation of a Kr $3d$ (or Xe $4d$) electron to an unoccupied np (Kr $n \geq 5$, Xe $n \geq 6$) orbital using linearly polarized synchrotron radiation leaves the excited atom fully aligned. The resulting excited state will undergo nonradiative decay often referred to as resonant Auger decay [1]. During this decay the alignment is shared between the resulting ion and the Auger electron, which results in, for example, an anisotropic distribution of Auger electrons. This kind of resonant atomic photoionization allows the study of the photon-atom interaction as well as the interactions within the many-electron atom after excitation. The resonant Auger spectra following the $3d(4d) \rightarrow np$ excitation in Kr (Xe) have been extensively studied for a couple of decades both experimentally and theoretically (see Ref. [1], and references therein).

The measurement of the intensity (relative or absolute cross section), angular distribution, and spin polarization of the resonant Auger electrons gives detailed information about the resonant Auger process. However, it has been shown that the parameters describing the angular distribution and the spin polarization of photoelectrons are not independent of each other for Auger decay from a state for which the total angular momentum $J=1$ [2]. Therefore a complete characterization of the resonant Auger process is not possible by measuring only the Auger electron but additional information about the alignment of the ion is needed. The measurement of the fluorescence radiation induced by linearly (circularly) polarized photons gives access to the alignment (and orientation) of the radiating state [3]. Naturally, photon-induced fluorescence spectroscopy (PIFS) is applicable only for excited atomic or ionic states that radiate. Such is the case of the Kr $4p^45p$ and Xe $5p^46p$ states which are below the double ionization threshold and can deexcite only by fluorescence emission. A partial wave analysis based on the determination of the alignment and orientation of the ion has been performed for some Kr $4p^45p$ states [4,5] and combining these with the angular distribution or spin polarization of the Auger electrons a complete characterization of the resonance Auger process would be possible.

However, due to experimental difficulties, reports of angular distribution and spin polarization parameters of the Auger electrons are very rare, and instead of a complete characterization, the calculations are compared with the separate alignment and/or orientation of the ion, or the angular distribution of the Auger electron [6–9]. These have been compared with calculations where the resonant Auger process has been considered as a two-step process (excitation and Auger decay), whose limits in describing the resonant Auger process have long been known [1,10]. The computational descriptions incorporated the direct photoionization amplitudes together with the resonant Auger amplitudes and thus have made it possible to include the experimentally observed interference effects in the studies [11–14]. The anisotropy parameters are very sensitive to interference between the direct and resonance channels as well as to the interference (or coherence) between different resonance channels populating the same state [4,5,12–15]. Kr is especially suitable for interference investigations, since only the two resonances $3d_{3/2}^{-1}5p$ and $3d_{5/2}^{-1}6p$ overlap due to their lifetime broadening.

Recently, the excitation energy dependence of the intensity and angular distribution parameter of Auger electrons for the Kr $4p^4(^1D)np$ $(n=5,6)$ states across the $3d_{3/2}^{-1}5p$ and $3d_{5/2}^{-1}6p$ resonances was studied [13]. Here we study the fluorescence emitted from the $4p^4(^1D)5p$ states, and also the $3d_{5/2}^{-1}5p$ resonance. The high resolution of fluorescence spectroscopy allows the examination of those states that overlap in electron spectra and thus provides additional information. The basis set of the previous calculations [13] was extended and these new calculations are compared with the present experimental and earlier theoretical results. Moreover, the

*anna.sankari@oulu.fi

effects of the radiative cascades populating the $4p^4(^1D)5p$ states from the higher-lying states are discussed.

II. EXPERIMENT

The PIFS measurements were performed at the Gas Phase Photoemission beam line [16] of the ELETTRA storage ring in Trieste, Italy. In the experimental setup, the gas jet coming from a hypodermic needle crossed the photon beam perpendicularly. The fluorescence light emitted was collimated by a spherical mirror mounted in the perpendicular direction to both the photon beam and the gas jet and parallel to the electric vector of the incident radiation. The full angle of the acceptance cone was about 20°.

The emitted fluorescence was focused to the entrance slit of a Czerny-Turner type monochromator, manufactured by McPherson, and the dispersed light was detected by a liquid-nitrogen cooled charge-coupled device (CCD) camera (from Roper Scientific). Some second order light was observed at the detector, but no second order lines were found in the measured wavelength region. The fluorescence monochromator was positioned in the plane of the storage ring, with the entrance slit and the axis of the spectrometer along the polarization vector of incoming radiation.

The photon energy was scanned across the Kr $3d_{5/2}^{-1}5p$, $3d_{3/2}^{-1}5p$, and $3d_{5/2}^{-1}6p$ resonances (at $h\nu$=91.200, 92.425, and 92.560 eV, respectively [17]) with a step of about 10 meV and at each energy the fluorescence spectrum was recorded. The recording time was 100–120 s at each point. The photon bandwidth was estimated to be about 7 meV according to the absorption spectra measured in between the fluorescence measurements. This photon bandwidth is only a fraction of the lifetime broadening of the resonances which have been experimentally shown to be around 80 meV [18]. Thus the measurement was performed in the resonant Raman regime [1].

The pressure in the vacuum chamber was kept at 9×10^{-5} mbar; the local pressure in the interaction region was estimated to be 10–50 times higher. No changes in the relative intensities of the fluorescence lines were observed as the pressure was slowly raised up to the operating value. The variations in photon flux during the scans were corrected with the help of the photodiode current recorded simultaneously.

The measured fluorescence spectra of Kr in the wavelength regions of interest are shown in Fig. 1. The transitions are identified in Table I with the aid of the NIST database [19]. The spectra shown are in qualitative agreement with a published spectrum [4] and have been corrected for the spatial variation of the efficiency of the CCD detector. The resolution was about 0.5 nm full width at half maximum.

III. THEORY

The theoretical approach behind the present multiconfiguration Dirac-Fock (MCDF) calculations is essentially the same that was used in Refs. [12,13]. In this work we incorporated the $3d^{-1}5p$, $3d^{-1}6p$, and $3d^{-1}7p$ configurations (with the restriction J=1) in the calculation of the excited reso-

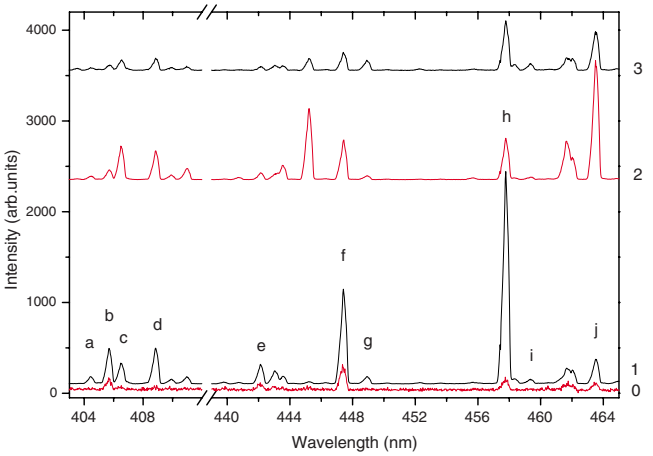

FIG. 1. (Color online) Spectra measured with a photon energy of (1) $h\nu$=91.200 eV (corresponding to the $3d_{5/2}^{-1}5p$ resonance), (2) $h\nu$=92.425 eV ($3d_{3/2}^{-1}5p$ resonance), (3) $h\nu$=92.560 eV ($3d_{5/2}^{-1}6p$ resonance), and (0) $h\nu$=80.0 eV (off-resonance): Spectra (3) and (0) have been multiplied by a factor of 2 and 10, respectively. For identification of the lines, see Table I.

nance state (R) using the GRASP92 package [20] to generate the wave functions. The resonant Auger final states (f) $4p^4np$ (n=5,6,7) were calculated together with the configurations $4s^{-1}4p^{-1}np$ and $4s^{-2}np$, also populated in the resonant Auger decay.

The intensity of the fluorescence emitted is determined by the optical transition probability between the initial and final states of the transition and thus it does not depend on the photon energy. Therefore, photon energy-dependent changes in the fluorescence intensity emitted from an initial state to some specific final states are considered to reflect the changes in the population and properties (such as alignment or orientation) of the initial state only (as assumed also in Refs. [4,5,14,15,21]). Thus, the changes in the fluorescence intensity from a resonant Auger final state are considered here to be directly proportional to the corresponding transition probability to the state. This approach, however, excludes the effects from radiative cascades. The photon en-

TABLE I. Identification and wavelengths of transitions shown in Fig. 1.

Label	Transition	Wavelength (nm) [19]
a	$4p^4(^1D)5p\ ^2D_{5/2}\rightarrow 4p^4(^1D)\ 5s\ ^2D_{3/2}$	404.466
b	$5p\ ^2P_{1/2}\rightarrow\ 5s\ ^2D_{3/2}$	405.704
c	$5p\ ^2D_{3/2}\rightarrow\ 5s\ ^2D_{3/2}$	406.513
d	$5p\ ^2D_{5/2}\rightarrow\ 5s\ ^2D_{5/2}$	408.834
e	$5p\ ^2P_{3/2}\rightarrow\ 5s\ ^2D_{3/2}$	442.272
f	$5p\ ^2P_{3/2}\rightarrow\ 5s\ ^2D_{5/2}$	447.501
g	$6s\ ^2D_{5/2}\rightarrow\ 5p\ ^2F_{7/2}$	448.988
h	$5p\ ^2F_{7/2}\rightarrow\ 5s\ ^2D_{5/2}$	457.721
i	$6s\ ^2D_{5/2}\rightarrow\ 5p\ ^2P_{3/2}$	459.280
j	$5p\ ^2F_{5/2}\rightarrow\ 5s\ ^2D_{3/2}$	463.389

ergy dependence of the fluorescence intensities was calculated exploiting the transition amplitude [22]

$$D(h\nu,f) = \langle f|\mathbf{D}|0\rangle + \sum_R \frac{\langle f|\mathbf{H}|R\rangle\langle R|\mathbf{D}|0\rangle}{h\nu - E_R + i\Gamma_R/2} \quad (1)$$

which accounts for interference between the direct photoionization channel (the first term) and the resonance channels (the second term). Experimental energies (E_R) and lifetime widths (Γ_R) of the resonances were adapted from Ref. [17] in the calculation of the denominator of the resonance term. The direct transition amplitudes $\langle f|\mathbf{D}|0\rangle$ were the same as in the earlier study [13]. As in Ref. [13], the excitation probabilities $\langle R|\mathbf{D}|0\rangle$ were calculated using REOS99 [23], but they were adjusted to correspond to the experimental values [17] to make the comparison with experiments easier, and to exclude any discrepancies stemming from the excitation step.

The resonant Auger transition probabilities, $\langle f|\mathbf{H}|R\rangle$, were calculated using the AUGER component [24] of the RATIP package [25]. The AUGER component does not include the shake transitions, which have been shown to play an important role in the resonant Auger decay of Kr [26]. The effects of the shake transitions (or relaxation), i.e., shake-down transitions $3d^{-1}mp \rightarrow 4p^4 5p$ ($m=6,7$), were included by estimating the transition probability from a resonance R to a final ionic state $|4p^4 5p, EJ\rangle$ (specified by the necessary quantum numbers EJ) [1,27]

$$\langle 4p^4 5p, EJ|\mathbf{H}|R\rangle_B = \sum_{n=5}^{7} \langle 5p|np\rangle\langle 4p^4 np, EJ|\mathbf{H}|R\rangle, \quad (2)$$

where the subscript B denotes the transition amplitude accounting for the shake transitions. The results of this approximation were denoted as B calculation in Ref. [13] and the same notation is used here together with a superscript n, which stands for new calculations. Thus, A (A^n) refers to (new) calculation without and B (B^n) with the shake transition, whereas A_d (A_d^n) and B_d (B_d^n) also include the contribution from the direct channel [in other words, the first term in Eq. (1)].

In Ref. [13], the computation did not include the $7p$ orbitals in the intermediate state ($3d^{-1}np$) or in the final ionic state ($4p^4 np$) and some of the discrepancies observed in comparison with the experimental results were attributed to the limited basis set used. Therefore new wave functions including the $7p$ orbital both in the intermediate and final states were calculated in order to see whether the incorporation of a higher ($7p$) orbital and additional configurations (i.e., $4s^{-1}4p^{-1}np$ and $4s^{-2}np$) improves the results as has been observed in, e.g., Ref. [21], where the inclusion of new configurations generally improved the agreement with experimental data although already the single-configuration model produced satisfactory results.

To estimate the radiative cascade contribution, Hartree-Fock (HF) calculations were performed using Cowan's code [28]. According to the dipole selection rules, the $4p^4 ns$, $4p^4(n-1)d$ ($n \geq 6$) and $4s^{-1}4p^{-1}5p$ configurations can populate the $4p^4(^1D)5p$ states. Some of the $4p^4 4d$ states lie higher than the $4p^4(^1D)5p$ states and they can contribute to the cascades too. The probabilities for these transitions were calculated as well as the decay rate of the $4p^4(^1D)5p$ states further to the $4p^4 5s$ and $4p^4 4d$ states.

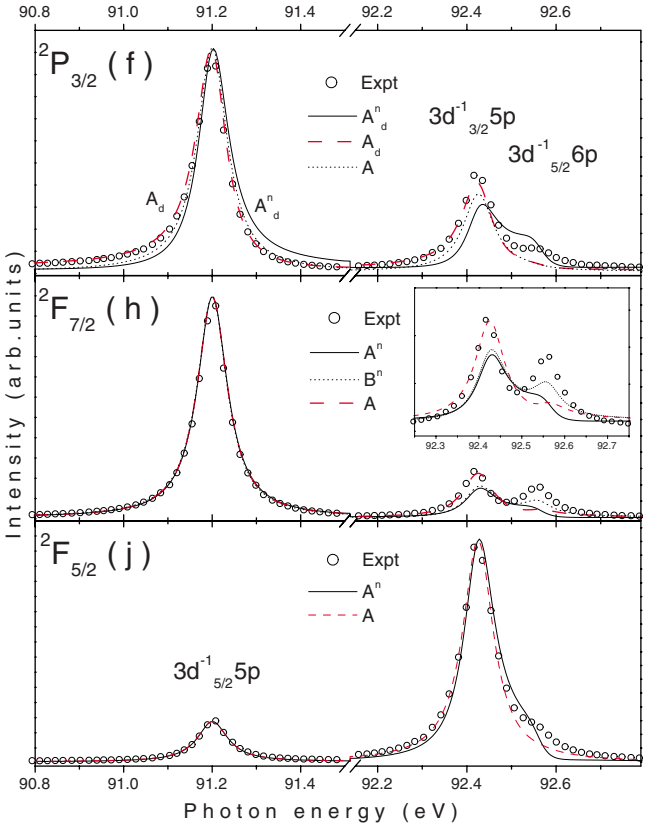

FIG. 2. (Color online) Intensities of lines f, h, and j as a function of excitation energy: Only every other experimental data point is shown for clarity. Inset in the middle panel shows the magnification of line h in the region of the overlapping resonances. For identification of the transitions, see Table I. Calculations with different approximations are also shown (see text for details).

IV. RESULTS AND DISCUSSION

A. Energy dependence of the fluorescence intensities

Figures 2 and 3 show the photon energy dependence of the fluorescence emitted from all the $4p^4(^1D)5p$ states. For each state the most prominent transition was selected from the measured wavelength regions. The selected transitions were confirmed to be the dominating deexcitation pathways of these states by our HF calculations. The chosen transitions correspond to lines b, c, d, f, h, and j, and the related final states as well as the wavelengths are given in Table I.

Lines f, h, and j in Fig. 2 correspond to transitions from the $4p^4(^1D)5p\ ^2P_{3/2}$, $^2F_{7/2}$, and $^2F_{5/2}$ final states, respectively. These states are also resolved in the electron spectrum and so they can be compared with the earlier study [13]. The energy dependence of the alignment and orientation parameters of lines f and h (as well as d) has also been investigated earlier [4,5]. Line f, due to emission from the $4p^4(^1D)5p\ ^2P_{3/2}$ state, shows the most prominent effect of extended calculations. The increase of the intensity at the $6p$

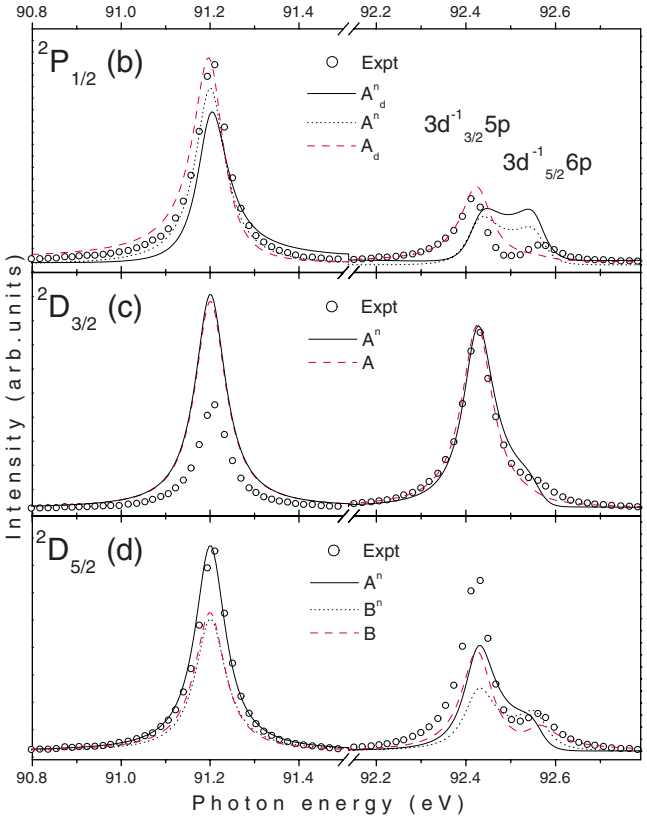

FIG. 3. (Color online) Intensities of lines b, c, and d as a function of excitation energy: Only every other experimental data point is shown for clarity. For identification of the transitions, see Table I. Calculations with different approximation are also shown (see text for details).

resonance is clearly seen by comparing the new A^n_d and old A_d results in the energy region of the overlapping resonances. The inclusion of shake transitions (the B approximation, results not shown) enhances the intensity at the $6p$ resonance even further [13]. The A^n_d and A_d are shown together with the old A calculation, which did not include the direct channel, so that the difference between the calculations A and A_d shows the effect of the direct contribution. As clearly seen from Fig. 2, the asymmetric Fano profile of the intensity reproduced by the new calculation (with the direct channel) at the first resonance is opposite to the experimental and previously calculated intensities; this is also observed for the other $4p^4(^1D)5p$ states (with $J \leq 3/2$). Previously [13], the direct contribution was observed to be too large for this state and the present comparison confirms this observation.

The calculation of the direct channel in Ref. [13] did not give any contribution at all for ionic states with $J > 3/2$. This applies also to the states $^2F_{7/2}$ and $^2F_{5/2}$ (initial states for fluorescence transitions h and j) even though Fig. 1 shows a clear direct contribution in the off-resonance spectrum for both states. The experimental intensities from these states are compared with the calculations from the old and new A approximations. In the case of line j, incorporating the shake transitions has no visible effect on the line shapes; therefore, the B calculations are not shown. The effect of inclusion of shake transitions is more pronounced for line h (calculation B^n). However, for both lines h and j the new calculations seem to predict more constructive interference between the overlapping resonances than observed experimentally or predicted earlier (A) for line h.

Figure 3 shows the fluorescence lines b, c, and d emitted by transitions from the $4p^4(^1D)5p\ ^2P_{1/2}$, $^2D_{3/2}$, and $^2D_{5/2}$ states, respectively. To estimate the energy separations of these almost degenerate resonant Auger final states it is convenient to use the wavelengths of lines a, b, and c (d has a different final state; see Table I). The energy separations of these states are 1.238 nm (a,b) and 0.808 nm (b,c), corresponding to 9.4 and 6.1 meV, respectively. In electron spectroscopy, the Doppler broadening for these states would be approximately 10 meV [29].

As can be seen from Fig. 3 the energy behavior of the three lines b, c, and d differs considerably. The gross dependence of their total intensity as a function of the photon energy across the overlapping resonances (measured in Ref. [13]) resembles mostly the energy behavior of line c with only a small shoulder at the third resonance. These fluorescence spectra allow the determination of the energy separation of these resonant Auger final states, but to deduce the relative intensity ratios of these states would require the detection of all lines from the states. Nonetheless, the lines (b–d) can provide information about the differing interference effects on their initial states.

In the case of line c [transition from the $4p^4(^1D)5p\ ^2D_{3/2}$ state], the effects of interference with both the direct channel and the other resonance channels are modest and hence only the results of the calculations A^n and A (both without any interference) demonstrate the effect of the larger basis set. The inclusion of shake transitions enhances slightly the intensity at the third resonance, as expected. The effect of the larger basis set is once again seen as a more pronounced $6p$ contribution and as a constructive interference between the overlapping resonances that appears to be too strong. For line c, the direct contribution does not have a clear effect on the energy dependence of the intensity even though it was not negligible in magnitude. Line b exhibits the same reversed asymmetry as line f in the A^n_d calculation including the direct channel. The old calculation (A_d) reproduced the asymmetric behavior fairly well, but could not predict enough intensity at the $6p$ resonance even with the approximation accounting for the shake transitions. For both lines b and d, the new calculation overestimates the intensity at the $6p$ resonance even without any additional shake contributions. In addition, the new calculations predict a constructive interference between the overlapping resonances, as deduced from the valley between the resonances [10], whereas the experimental (as well as the old calculated) intensities exhibit a destructive interference for both lines b and d.

There are two significant shortcomings in our new calculations. First, the contribution of the $3d^{-1}_{5/2}6p$ resonance is overestimated for all states except the $^2F_{7/2}$ state (line h). Second, reversed interference effects (constructive interference where it should be destructive and vice versa) are seen for both interference mechanisms accounting for other resonant or direct contributions. This is especially clear in the case of lines b and d (for interference between overlapping resonances) and lines b and f (for interference with the direct channel).

Since the direct amplitudes used here are the same as in the old calculations (predicting the correct interference behavior), the difference between the new and old calculations must stem from the resonant part of Eq. (1). A closer inspection of the resonant Auger final states $[4p^4(^1D)5p]$ reveals that the incorporation of the $7p$ orbital and higher configurations does not change much the composition (the mixing coefficients and configuration state functions) of the states. In contrast, the inclusion of the $7p$ orbital in the excited initial state $(3d^{-1}np)$ has a drastic effect on the mixing of these states and, further, on the transition amplitudes of the resonant Auger decay. Therefore, the deficiencies seen in our new calculations can be regarded as consequences of the initial state configuration interaction (ISCI) and these results underline the importance of the proper description of the excited state in this kind of calculations.

The preceding discussion is limited mainly to the shapes of the lines. The reason for this is that the measurements were performed in the collinear direction with the electric vector of the incident radiation. In this cylindrically symmetric geometry, we are not sensitive to polarization. The alignment of the initial state changes as the exciting energy is scanned across the resonances [see Ref. [5] for the $4p^4(^1D)\ ^2P_{3/2}$ state, Ref. [4] for the $^2D_{5/2}$ and $^2F_{7/2}$ states, and Ref. [15] for the $^2D_{3/2}$ state], so that the alignment-dependent angular distribution [21,30] of the emitted radiation changes. This is reflected in the intensities at the resonances and a variation is observed for the fluorescence emitted by transitions from the same initial state to final states with different total angular momenta, since the angular distribution of the fluorescence radiation depends on a coefficient containing the total angular momenta of both the initial and final states.

B. Radiative cascades

The presence of the cascade contribution, which has not been removed from the experimental results, should also be considered. The radiative cascades from higher-lying configurations reflect the increasing population of the states as the excitation energy increases. This can be seen from Fig. 4 where the photon energy dependence of the transitions f and h are shown together with the photon energy dependence of related cascade transitions. The upper panel shows a cascade transition populating the $^2P_{3/2}$ state (weaker line i) and the fluorescence emitted from the same $^2P_{3/2}$ state, which also includes the cascade transition shown (note different scales). The lower panel shows the same for the $^2F_{7/2}$ state. The contribution of the cascade transitions is not a constant but changes as a function of excitation energy and has the strongest impact at the third resonance.

Although electron spectra usually suffer from poor resolution in comparison with fluorescence spectra, the electron spectra are entirely free from cascade contributions, which is the main drawback of PIFS [31,32]. A proper interpretation of the fluorescence requires the isolation of the cascade contribution either by measuring all cascade lines contributing to the state or by comparing the same information obtained from electron spectra as discussed in Ref. [32]. As mentioned

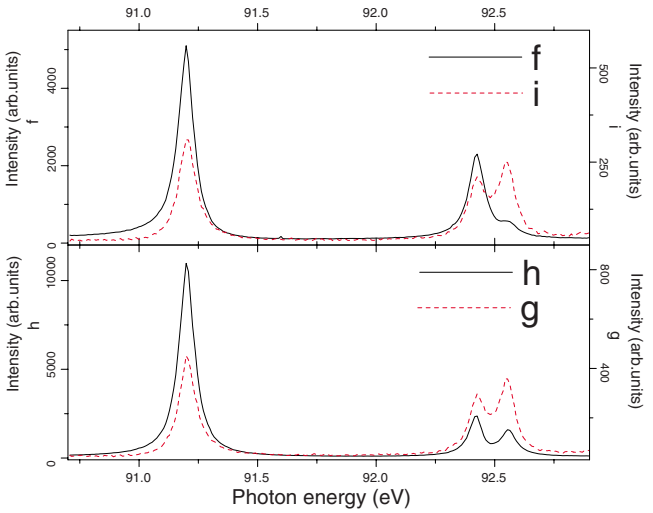

FIG. 4. (Color online) Photon energy dependences of (i) $6s\ ^2D_{5/2}\rightarrow 5p\ ^2P_{3/2}$ (dashed line) and (f) $5p\ ^2P_{3/2}\rightarrow 5s\ ^2D_{5/2}$ (solid line) transitions (upper panel) and (g) $6s\ ^2D_{5/2}\rightarrow 5p\ ^2F_{7/2}$ (dashed line) and (h) $5p\ ^2F_{7/2}\rightarrow 5s\ ^2D_{5/2}$ (solid line) transitions (lower panel). Solid curves represent the energy dependence of the fluorescence coming from the investigated $4p^4(^1D)5p$ states (left scales) whereas dashed curves show the behavior of the cascades (right scales).

earlier, a direct comparison between electron spectra and the present fluorescence spectra is possible only for the $4p^4(^1D)5p\ ^2P_{3/2}$, $^2F_{5/2}$, and $^2F_{7/2}$ states. Nevertheless, the comparison in the region of the overlapping resonances revealed that the only difference is the more pronounced $6p$ resonance. This can be attributed to the cascade contribution, which is stronger at the $6p$ resonance as shown in Fig. 4.

No visible differences in the asymmetry of the profiles were observed in the comparison of the electron and fluorescence spectra, which justifies the assumption of the isotropic contribution of the radiative cascades made, e.g., in Refs. [4,5,9,14,15,21]. This has also been verified by measuring the polarization of some cascade lines [9]. The loss of anisotropy has been shown for the second step Auger lines [6] and additional cascade steps are expected to decrease the anisotropy even further.

The amount of the cascade contribution has earlier been estimated by an extensive set of calculations including several configurations as well as single and double excitations [9] or via a transition arrays technique [4,5,8,14,15] together with the inspection of the experimental fluorescence spectra in order to estimate which transitions are responsible for the dominant cascade contribution. According to the latter studies, the major contributions are from the $4p^4(^1D)6s\ ^2D_{5/2}$ [to the $4p^4(^1D)5p\ ^2P_{3/2}$ [5], $^2F_{7/2}$, and $^2D_{5/2}$ states [4]] and $4p^4(^1D)6s\ ^2D_{3/2}$ $(\rightarrow ^2P_{3/2}$ [4]) states as well as from the $4p^4(^1D)5d\ ^2G_{9/2}$ state $(\rightarrow ^2F_{7/2}$ [4]). According to our HF calculations, the $(^1D)6s\ ^2D_{3/2,5/2}$ states have the largest transition probability from the $4p^4ns$ $(n>5)$ states to the $4p^4(^1D)5p$ states. However, our calculations also show that the most probable dipole-allowed transitions would be from the $4s^{-1}4p^{-1}5p$ states and the transitions from the $4p^4(n-1)d$ states would be more probable than transitions from a

$4p^4ns$ initial state. Of course, even the highest transition probability will not have any influence if the state is not populated or the state decays dominantly via some other transition. For example, for the $4s^{-1}4p^{-1}5p$ states the second step Auger decay is energetically possible and most of these states (99.99% predicted by our calculations) will decay via Auger electron emission. However, the lifetime of the $4s^{-1}4p^{-1}5p$ states is much shorter than the lifetime of the $4p^4(^1D)5p$ states and, as the most populated states in the resonant Auger spectrum, they could make some contribution to the $4p^4(^1D)5p$ states as well.

The shake-up process is considered as the dominant source of the cascade transitions (see, e.g., Ref. [4]). However, as discussed already in the case of Xe [9], the resonant Auger spectrum also contains the conjugate shake-up satellite lines such as $5p^47s$, $6d$ in Xe. The corresponding $4p^46s$, $5d$ satellite lines in Kr are also observed in the $4s$ photoelectron spectrum measured with photon energies below the $3d \rightarrow np$ excitations [33]. These states are thus populated both directly and via a fluorescence transition ($4p^46p/7p \rightarrow 4p^45d/6s$) following a shake-up process. The population mechanism of these states is not important as long as the isotropy of the fluorescence emitted in the transition to the investigated $4p^45p$ state is checked. However, this should be done for all the contributing cascades and since some of the cascades fall into regions of infrared or vacuum ultraviolet radiation the determination of their contributions would require a different experimental setup and would therefore be a very tedious task.

V. CONCLUSIONS

The photon energy dependence of the fluorescence emitted from the Kr $4p^4(^1D)5p$ states was measured in the energy region of the first three $3d^{-1}np$ resonances. The results were compared with the MCDF calculation including the interference effects originating from the contribution of the direct channel and other resonance channels and discussed together with the corresponding electron spectra published recently [13]. The comparison between the experimental intensities and theoretical predictions showed how the initial state configuration interaction (ISCI) can have a strong influence on interference effects calculated for the energy dependence of the population of the $4p^4(^1D)5p$ states.

ACKNOWLEDGMENTS

A.S. acknowledges financial support from the Finnish Cultural Foundation. R.S. acknowledges financial support from the Helsingin Sanomat. A.S. and R.S. gratefully acknowledge the hospitality of the Gas Phase Beamline group in ELETTRA during their stay there.

[1] G. B. Armen, H. Aksela, T. Åberg, and S. Aksela, J. Phys. B **33**, R49 (2000).
[2] N. M. Kabachnik and A. N. Grum-Grzhimailo, J. Phys. B **34**, L63 (2001).
[3] C. H. Greene and R. N. Zare, Annu. Rev. Phys. Chem. **33**, 119 (1982).
[4] K.-H. Schartner, R. H. Schill, and D. Hasselkamp, S. Mickat, S. Kammer, L. Werner, S. Klumpp, A. Ehresmann, H. Schmoranzer, B. M. Lagutin, and V. L. Sukhorukov, J. Phys. B **38**, 4155 (2005).
[5] K.-H. Schartner, R. Schill, D. Hasselkamp, S. Mickat, S. Kammer, L. Werner, S. Klumpp, A. Ehresmann, H. Schmoranzer, B. M. Lagutin, and V. L. Sukhorukov, J. Phys. B **40**, 1443 (2007).
[6] M. Kitajima, M. Okamoto, Y. Shimizu, H. Chiba, S. Fritzsche, N. M. Kabachnik, I. P. Sazhina, F. Koike, T. Hayaishi, H. Tanaka, Y. Sato, and K. Ueda, J. Phys. B **34**, 3829 (2001).
[7] B. Zimmermann, O. Wilhelmi, K.-H. Schartner, F. Vollweiler, H. Liebel, A. Ehresmann, S. Lauer, H. Schmoranzer, B. M. Lagutin, I. D. Petrov, and V. L. Sukhorukov, J. Phys. B **33**, 2467 (2000).
[8] B. M. Lagutin, I. D. Petrov, Ph. V. Demekhin, V. L. Sukhorukov, F. Vollweiler, H. Liebel, A. Ehresmann, S. Lauer, H. Schmoranzer, O. Wilhelmi, B. Zimmermann, and K.-H. Schartner, J. Phys. B **33**, 1337 (2000).
[9] M. Meyer, A. Marquette, A. N. Grum-Grzhimailo, U. Kleiman, and B. Lohmann, Phys. Rev. A **64**, 022703 (2001).
[10] E. Kukk, H. Aksela, A. Kivimäki, J. Jauhiainen, E. Nõmmiste, and S. Aksela, Phys. Rev. A **56**, 1481 (1997).
[11] S. L. Sorensen, T. Åberg, J. Tulkki, E. Rachlew-Källne, G. Sundström, and M. Kirm, Phys. Rev. A **50**, 1218 (1994).
[12] S. Fritzsche, J. Nikkinen, S.-M. Huttula, H. Aksela, M. Huttula, and S. Aksela, Phys. Rev. A **75**, 012501 (2007).
[13] A. Sankari, S. Alitalo, S. Fritzsche, J. Nikkinen, A. Kivimäki, S. Aksela, and H. Aksela, Phys. Rev. A **76**, 022702 (2007); **76**, 069902(E) (2007).
[14] B. M. Lagutin, I. D. Petrov, V. L. Sukhorukov, S. Kammer, S. Mickat, R. Schill, K.-H. Schartner, A. Ehresmann, Yu. A. Shutov, and H. Schmoranzer, Phys. Rev. Lett. **90**, 073001 (2003).
[15] B. M. Lagutin, I. D. Petrov, V. L. Sukhorukov, Ph. V. Demekhin, B. Zimmermann, S. Mickat, S. Kammer, K.-H. Schartner, A. Ehresmann, Yu. A. Shutov, and H. Schmoranzer, J. Phys. B **36**, 3251 (2003).
[16] K. C. Prince, R. R. Blyth, R. Delaunay, M. Zitnik, J. Krempasky, J. Slezak, R. Camilloni, L. Avaldi, M. Coreno, G. Stefani, C. Furlani, M. de Simone, and S. Stranges, J. Synchrotron Radiat. **5**, 565 (1998).
[17] G. C. King, M. Tronc, F. H. Read, and R. C. Bradford, J. Phys. B **10**, 2479 (1977).
[18] O.-P. Sairanen, A. Kivimäki, E. Nõmmiste, H. Aksela, and S. Aksela, Phys. Rev. A **54**, 2834 (1996).
[19] NIST Atomic Spectra Database, http://physics.nist.gov/PhysRefData/ASD/
[20] F. A. Parpia, C. Froese Fischer, and I. P. Grant, Comput. Phys. Commun. **94**, 249 (1996).
[21] P. O'Keeffe, S. Aloïse, S. Fritzsche, B. Lohmann, U. Kleiman, M. Meyer, and A. N. Grum-Grzhimailo, Phys. Rev. A **70**, 012705 (2004).

[22] T. Åberg and G. Howat, in *Corpuscles and Radiation in Matter I*, edited by S. Flügge and W. Mehlhorn, Vol. 31 of Handbuch der Physik (Springer, Berlin, 1982), p. 469.
[23] S. Fritzsche, C. Froese Fischer, and C. Z. Dong, Comput. Phys. Commun. **124**, 340 (2000).
[24] S. Fritzsche, B. Fricke, and W.-D. Sepp, Phys. Rev. A **45**, 1465 (1992).
[25] S. Fritzsche, J. Electron Spectrosc. Relat. Phenom. **1155**, 114 (2001); Phys. Scr., T **T100**, 37 (2002).
[26] J. Jauhiainen, H. Aksela, O.-P. Sairanen, E. Nõmmiste, and S. Aksela, J. Phys. B **29**, 3385 (1996).
[27] S. B. Whitfield, J. Tulkki, and T. Åberg, Phys. Rev. A **44**, R6983 (1991).
[28] R. D. Cowan, *The Theory of Atomic Structure and Spectra* (University of California Press, Berkeley, 1981).
[29] P. Baltzer, L. Karlsson, M. Lundqvist, and B. Wannberg, Rev. Sci. Instrum. **64**, 2179 (1993).
[30] E. G. Berezhko and N. M. Kabachnik, J. Phys. B **10**, 2467 (1977).
[31] K.-H. Schartner, P. Lenz, B. Möbus, B. Magel, H. Schmoranzer, and M. Wildberger, Phys. Scr. **41**, 853 (1990).
[32] J. Jiménez-Mier, C. D. Caldwell, M. G. Flemming, S. B. Whitfield, and P. van der Meulen, Phys. Rev. A **48**, 442 (1993).
[33] A. Caló, S. Atanassova, R. Sankari, A. Kivimäki, H. Aksela, and S. Aksela, J. Phys. B **39**, 4169 (2006).